20

Giant planet, brown dwarf, and low-mass star interiors

W.B. HUBBARD

Department of Planetary Sciences, Lunar and Planetary Laboratory, University of Arizona, Tucson, AZ 85721, USA

Abstract

Astrophysical objects of low mass, ranging from giant planets to extreme dwarf main-sequence stars, have a number of physical characteristics in common due to properties of their equations of state. Their luminosities are low (much less than the solar luminosity $L_\odot$) and their evolutionary timescales are typically measured in Gyr. So far there are few observational examples of these objects, although they are undoubtedly numerous in the galaxy. The lower mass limit is set by the object's ability to retain hydrogen during accumulation (about the mass of Saturn), while the upper mass limit is set by the lifting of electron degeneracy by high internal temperature. Objects confined within this broad range, which extends up to about 0.1 $M_\odot$, are governed by the thermodynamics of liquid metallic hydrogen. In this paper, we discuss the implications of this feature of their interior structure for their radii, interior temperatures, thermonuclear energy generation rates, and luminosities. We conclude with a brief assessment of the confrontation between observations and theory in galactic clusters and in the solar system.

L'équation d'état des corps célestes de faible masse, qui vont des planètes géantes aux étoiles naines qui sont à la limite de la séquence principale, est a l'origine d'un ensemble commun de propriétés physiques. Leur luminosité est de beaucoup inférieure à celle du Soleil et leur temps caractéristique d'évolution se mesure en milliards d'années. A ce jour, nous ne connaissons que quelques exemples de ces objets malgré la conviction qu'ils sont nom-

https://doi.org/10.1017/S0252921100026488 Published online by Cambridge University Press

breux dans la Galaxie. La limite inférieure en masse (approximativement la masse de Saturne) est fixée par la capacité de retenir l'hydrogène au cours du processus d'accumulation de la matière. La limite supérieure est atteinte lorsque la température interne est suffisamment élevée pour que les electrons ne soient plus dégénérés (environ 0.1 $M_\odot$). Les propriétes des corps qui se retrouvent dans ce domaine étendu en masse sont principalement déterminées par la thermodynamique de l'hydrogène métallique liquide. Cet article présente les effets de ce point commun de leur structure interne sur leurs rayons, leurs température internes, leurs taux de génération d'énergie thermonucléaire et leurs luminosités. Nous concluons par une brève discussion de la confrontation entre les observations et la théorie dans le cas des amas galactiques ainsi que dans le système solaire.

20.1 Introduction

In this chapter, we shall discuss the implications of the equation of state (mainly that of hydrogen) for giant planets, brown dwarfs, and very low-mass stars. Although the mass range covered by these seemingly disparate objects is moderately large (about two orders of magnitude), the physics of the equation of state is basically the same, and leads to certain common characteristics.

By *giant planet*, we mean the four largest planets of the solar system, Jupiter, Saturn, Uranus, and Neptune, as well as their so far hypothetical counterparts in other solar systems. The equation of state of hydrogen is particularly relevant to the largest two giant planets, Jupiter and Saturn. Giant planets have masses M which lie in the range $5 \times 10^{-5} M_\odot \leq M \leq 1 \times 10^{-3} M_\odot$ ($M_\odot$ = mass of the sun).

The term *brown dwarf* (BD) has become standard usage for designating a class of hydrogen-rich objects with the following characteristics: (a) composition similar to the sun, i.e. dominated by hydrogen; (b) masses about ten times larger than that of Jupiter; (c) masses smaller than the critical mass for sustained thermonuclear fusion of hydrogen. Masses of brown dwarfs lie roughly in the range $1 \times 10^{-2} M_\odot \leq M \leq 1 \times 10^{-1} M_\odot$. At present there is some uncertainty about the possible modes of origin of objects in the mass range $1 \times 10^{-3} M_\odot \leq M \leq 1 \times 10^{-2} M_\odot$; such objects could be considered either very large giant planets or extremely small BD's. According to Boss (1986), the minimum mass for direct formation of a BD from collapse of an interstellar cloud of H and He is $\sim 0.02 M_\odot$, and objects of lower mass form through a different sequence of events, which begins with coagulation of planetesimals from solid particles. As we shall discuss, these lower mass

https://doi.org/10.1017/S0252921100026488 Published online by Cambridge University Press

objects lie below the critical mass for fusion of deuterium and it is therefore convenient to classify them as giant planets (GP's) rather than BD's.

Objects which are more massive than $\sim 10^{-1} M_\odot$ but still substantially less massive than the sun are termed very low mass stars (VLM), or extreme M dwarfs. In contrast to the situation for GP's and BD's, many observational examples of VLM's exist.

All of the objects under discussion here, GP's, BD's, and VLM's, have intrinsic luminosities L which are small compared with the luminosity of the sun $L_\odot$. Their luminosity and associated interior thermal state change very slowly with time, typically over time scales measured in Gyr. At the same time, depending on the relative efficiency with which these objects are formed, they may comprise an appreciable fraction of the mass of the Galaxy. This mass could thus be largely hidden in objects which are difficult to detect.

In modeling objects across the indicated mass range, we assume that the composition is similar to that of the sun, i.e., predominantly hydrogen. Although there is some uncertainty about the precise composition and indeed there may be some variation with mass and age, for our purposes it is sufficient to take a uniform composition with a helium mass fraction $Y = 0.25$, and a hydrogen mass fraction $X = 1 - Y - Z$, where Z is the mass fraction of all elements heavier than helium (the so-called metals). The value of Z plays little or no role in the equation of state as it does not exceed 0.02 for solar composition. However, the value of Z affects photon opacities in the outermost layers of these hydrogen-rich objects, and hence has a large impact on their interior thermal state. In the lowest mass range, $M \lesssim 3 \times 10^{-4} M_\odot$, significant amounts of hydrogen are lost during accumulation of the object, and Z becomes large enough to play a significant role in the equation of state.

The similarity of the physics of the equation of state in all of these objects ultimately arises from the fact that their interiors lie for the most part within the following limits:

$$\theta = \epsilon_F / kT \gg 1 \tag{1}$$

and

$$\Gamma = e^2 / akT \gg 1 \tag{2}$$

Here θ is the electron degeneracy parameter, the ratio of the electron fermi energy ϵ_F to a typical thermal excitation energy kT. Similarly, the ion

coupling parameter (which for hydrogen is the same as the electron coupling parameter) Γ measures the ratio of a typical ion coulomb energy e^2/a to kT. Here e is the ion charge and a is the average distance between ions. Because both of these parameters are large, the object's equation of state is mainly governed by the physics of metallic hydrogen. And, because Γ typically lies in the range $1 < \Gamma < 100$, the metallic hydrogen is in a strongly coupled liquid phase.

A third dimensionless parameter of relevance to the equation of state is the density parameter $r_s = a/a_0$, where a_0 is the Bohr radius. This parameter ranges from $r_s \approx 1$ for a giant planet such as Jupiter to $r_s \approx 0.1$ for the most massive BD's. Under these circumstances, the relation between pressure P and mass density ρ is largely independent of temperature T, and can be expressed in the form

$$P \sim \rho^{\alpha} \tag{3}$$

with $1.6 < \alpha < 2$. This result is universally true for hydrogen-rich objects in the relevant mass range, and leads to the remarkable result that such objects have very similar radii R, regardless of their mass. However, this similarity does not extend to quantities related to the object's interior thermal state, such as its total intrinsic luminosity L, its effective temperature T_e, and its central temperature $T_{\rm central}$, which in general depend sensitively on both the mass and age of the object.

Some of these points are illustrated in Table 1.1, in which we compare Jupiter, a well-studied metallic-hydrogen object with an age of about 5 Gyr, with a hypothetical BD of the same age and gross chemical composition. Since Jupiter rotates rapidly and is therefore nonspherical, the radius R which is given is the equatorial radius at the 1-bar pressure level. For Jupiter, the quantity $\rho_{\rm central}$ is actually the highest density of the metallic hydrogen zone in the planet's interior, and does not refer to the density of a Z-rich central core.

20.2 Radius vs. mass; relation to equation of state

The overall behavior of the $R(M)$ curve for giant planets, BD's, and VLM's is extremely diagnostic of the equation of state of metallic hydrogen-helium mixtures, and its general shape is shown in Figs. 1.1 and 1.2.

Figure 1.1 shows a maximum radius for solar composition of 75740 km at $M = 0.004 M_\odot$ (about four Jupiter masses). For pure hydrogen, the maximum in $R(M)$ moves to $0.006 M_\odot$ and 87200 km. The maximum radius exists as a direct consequence of a competition between electrostatic con-

https://doi.org/10.1017/S0252921100026488 Published online by Cambridge University Press

Table 20.1. ***Comparison between Jupiter and a typical brown dwarf***

	Jupiter	brown dwarf
$M(\odot)$	0.001	0.070
R (km)	71492 ± 4	55870
age (Gyr)	5	5
$L/L_\odot$	0.9×10^{-9}	1.5×10^{-5}
$L_{\rm nuclear}/L$	0	0.28
T_e	124 K	1262 K
T (10 bar)	337 K	550 K
$\rho_{\rm central}$	4 g cm^{-3}	979 g cm^{-3}
$T_{\rm central}$	22600 K	1.683×10^6 K

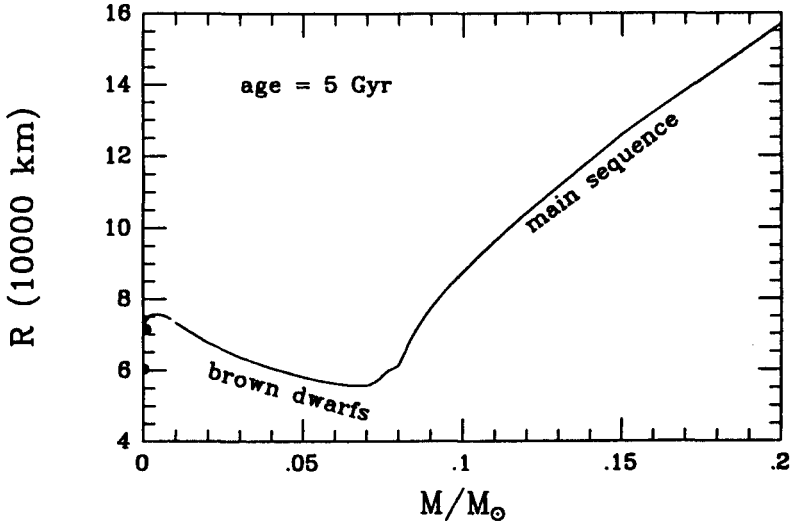

Fig. 20.1 Solid line (—): radius vs. mass for solar-composition objects at a cooling age of 5 Gyr. Objects to the left of the short break at $0.01M_\odot$ are considered giant planets. BD's extend from the break to $0.08M_\odot$. •: GP's, shown in more detail in Fig. 1.2.

tributions to the equation of state which contribute a negative component to the pressure, and the electron fermi pressure, which contributes positively. For $M < 0.004M_\odot$ ($r_s \sim< 0.6$) the electrostatic contributions to the pressure are sufficiently important (pressure increases sufficiently rapidly with increasing density) that there is a positive slope to the $M(R)$ curve in this mass range. For masses greater than $0.004M_\odot$, the degenerate electron fermi pressure begins to dominate the equation of state, causing a decrease in R with increasing M. As Fig. 1.1 shows, there is a minimum in the $R(M)$ curve at about $0.07M_\odot$. The minimum is not especially related to the equation of state, but is instead produced by the onset of thermonuclear energy

https://doi.org/10.1017/S0252921100026488 Published online by Cambridge University Press

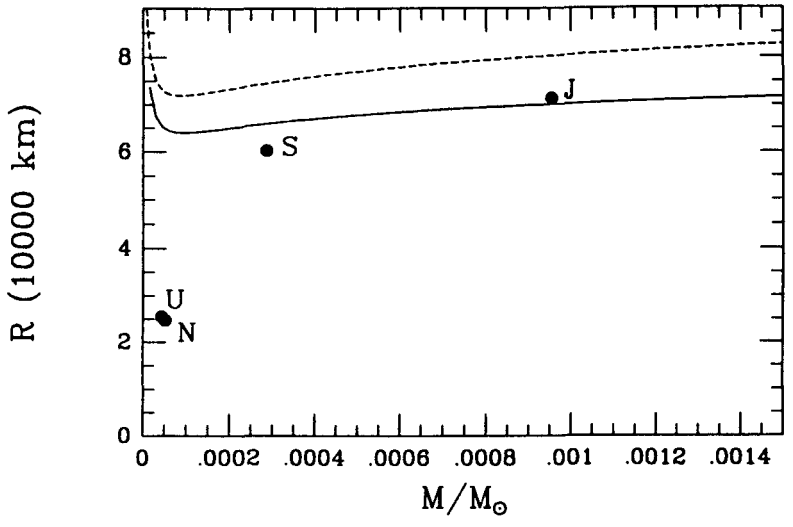

Fig. 20.2 Solid line (—): radius vs. mass for spherically symmetric solar-composition objects at a finite interior temperature. Dashed line (– – –): same, but for pure H. •: giant planets Jupiter, Saturn, Uranus, Neptune.

generation in the BD's core, which tends to raise the interior temperature and reduces the electron degeneracy. According to Burrows et al. (1993), the minimum mass for sustained thermonuclear energy generation in BD's is $0.0767 M_\odot$; objects which are more massive are not BD's but are instead VLM's, and settle eventually on the main sequence. The minimum in $R(M)$ lies slightly below this minimum mass because Fig. 1.1 is computed for a finite age of 5 Gyr, and the most massive BD's are able to burn hydrogen for several Gyr before they fail to settle on the main sequence.

Figure 1.2 shows an expanded view of the extreme left-hand corner of Fig. 1.1. The solid curve again shows $R(M)$ for solar-composition material, calculated for temperatures along an adiabatic compression curve corresponding to the interiors of Jupiter and Saturn, while the dashed curve is the same, but for pure hydrogen. At masses slightly below the mass of Saturn ($0.0003\ M_\odot$), the metallic-hydrogen core vanishes, and $R(M)$ is determined by the equation of state of dense molecular hydrogen. At masses slightly below the mass of Uranus or Neptune ($5 \times 10^{-5} M_\odot$), the molecular hydrogen adiabat falls entirely in the ideal-gas region, and as a result $R(M)$ begins to increase with falling mass. However, the latter behavior cannot be realized in nature. As Fig. 1.2 makes clear, giant planets less massive than Saturn cannot capture significant amounts of hydrogen when they are formed, and their interior equations of state are dominated by heavier nuclei. More detailed analysis of the interior compositions of Jupiter and Saturn (Chabrier et al., 1992) shows that both are more enriched in the Z-component than

solar composition, with Saturn more enriched than Jupiter. In Fig. 1.2, Jupiter plots slightly above the solar-composition curve because correction for rotation of Jupiter has not been included in the solid curve; when this correction is included, Jupiter plots slightly below the theoretical curve for solar composition.

20.3 Variation of luminosity with mass

The heat flow which corresponds to the observed luminosity L is presumed to be derived from two sources: (a) heat release from the object due to work done on the object's interior and due to changes in internal energy E; (b) heat release due to nuclear reactions in the object's interior. Both of the sources can be combined into the equation

$$L = \int_0^M \frac{P}{\rho^2}\frac{d\rho}{dt}dm - \frac{d}{dt}\int_0^M E dm + \int_0^M \epsilon_N(\rho,T)dm \qquad (3)$$

where dm is an element of mass, t is the time, and ϵ_N is the rate of release of energy by nuclear reactions. For the giant planets, ϵ_N is effectively zero because temperatures and densities are too low for fusion reactions to proceed, and the abundances of radioactive high-Z elements such as ^{40}K, ^{232}Th, and ^{238}U are too low for radioactive decay to be significant. In the giant planets, only the first two terms in Eq. 3 are important, although they must be carefully evaluated generalized in the case of Saturn to account for immiscibility of helium in liquid metallic hydrogen and consequent formation of a helium-enriched core (Stevenson, 1975).

As masses increase into the BD range, one must consider contributions to ϵ_N from the following reactions (Burrows et al., 1993):

$$p + p \rightarrow d + e^+ + \nu_e \qquad (1.442\ \text{MeV}) \qquad (4)$$

$$p + d \rightarrow {}^3\text{He} + \gamma \qquad (5.494\ \text{MeV}) \qquad (5)$$

In the BD mass range, these reactions stop at ^{3}He. In addition, the following reaction does not contribute significantly to ϵ_N but does serve as a useful tracer of BD evolution:

$$p + {}^7\text{Li} \rightarrow 2\alpha \qquad (6)$$

Basically, the division between VLM's and BD's is defined by reaction (4). For masses above the critical mass of $0.0767 M_\odot$, central densities exceed about 10^3 g cm^{-3}, and central temperatures exceed about 2×10^6 K. Under these circumstances, enough heat is liberated by reactions (4) and (5) to

https://doi.org/10.1017/S0252921100026488 Published online by Cambridge University Press

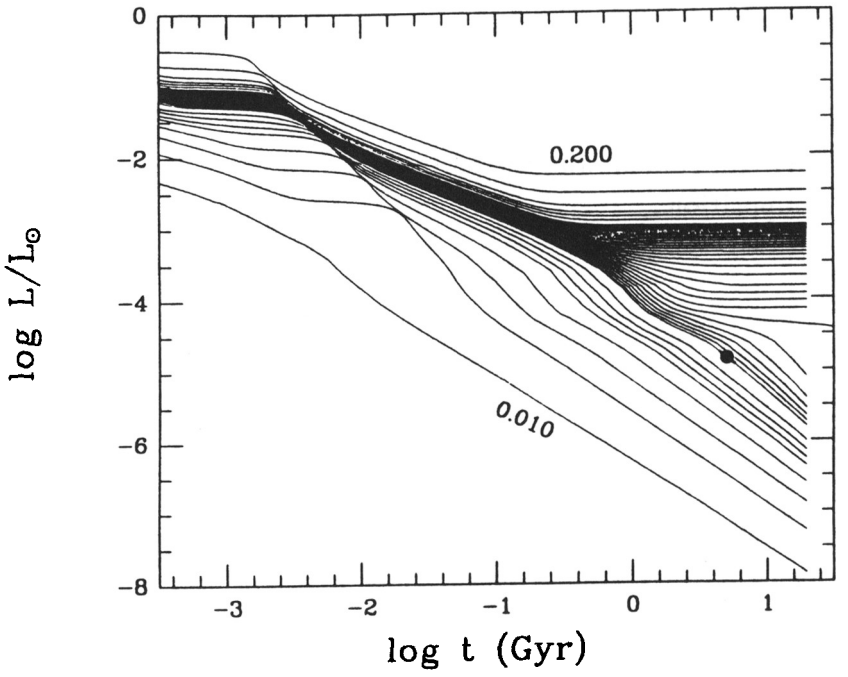

Fig. 20.3 Curves of luminosity vs. time for VLM's and BD's of various mass. The upper curve is for a VLM of $0.200M_\odot$, while the lowest curve is for $0.010M_\odot$. A smaller mass interval has been used for objects near the critical mass for hydrogen burning. • shows the $0.070M_\odot$ model presented in Table 1.1.

balance the heat radiated by the VLM's atmosphere. For objects below the critical mass, reaction (5) can still proceed but reaction (4) does not. As a result, the BD has a relatively brief phase during which it burns primordial deuterium, but once the deuterium is gone, only heat release from the first two terms of eq. (3) plays a role in the BD's luminosity. At the lower end of the BD mass range, even deuterium does not burn. This second critical mass lies at about $0.015M_\odot$ and corresponds to central densities about ~ 20 g cm^{-3}, and central temperatures $\sim 0.5 \times 10^6$ K. Objects below this second critical mass can be considered GP's.

Figure 1.3 illustrates the above-described effects, showing the evolution of luminosity with time on a double-logarithmic scale. The bifurcation of objects into VLM's and BD's at the right side of the figure is apparent. The model with the prolonged curve is just subcritical at $0.0765M_\odot$, and shows a gradual decline of luminosity with time over time periods longer than the age of the universe.

Other features in Fig. 1.3 are worthy of note. A "ripple" in $L(t)$ is apparent for $-3 < \log t < -1.5$, with the onset of the "ripple" progressively later for smaller masses. This "ripple" is caused by thermonuclear fusion of

https://doi.org/10.1017/S0252921100026488 Published online by Cambridge University Press

primordial deuterium via reaction (5), assuming that the primordial deuterium mass fraction is $Y_d = 2 \times 10^{-5}$. The "ripple" vanishes for masses between $0.010 M_\odot$ (lowest curve in Fig. 1.3) and $0.020 M_\odot$ (second lowest curve in Fig. 1.3). Thus the critical mass for deuterium burning lies at $M \approx 0.015 M_\odot$, and we conclude that GP's, such as Jupiter, will contain the primordial deuterium abundance, but BD's older than ~ 0.1 Gyr will be depleted in deuterium.

Another, fainter, "ripple" in Fig. 1.3 can be discerned at $L \sim 10^{-4} L_\odot$. This "ripple" is not related to the equation of state or to nuclear reaction rates, but is caused by temporarily increased atmospheric opacity at this luminosity level, as a consequence of the formation of dust grains in the BD's atmosphere at levels where most photons are just able to escape to space (Burrows et al., 1989). This increase in opacity causes the BD luminosity to temporarily drop and the cooling age of the BD to be correspondingly extended.

As Fig. 1.3 makes clear, L is a function of both M and t for BD's and VLM's, and thus identification of an object as a possible BD requires knowledge of its age as well as its luminosity. But there is, theoretically, an independent test which can be used to determine whether an object lies within the BD mass range. Fragile nuclei such as deuterium and lithium are destroyed via reactions (5) and (6) respectively, at significantly lower temperatures than those required for reaction (4) to proceed. We have already discussed the destruction of an initial deuterium component in a BD. The corresponding destruction of initial lithium requires a mass equal or greater than about $0.065 M_\odot$ (Magazzù, Martin, and Rebolo, 1993, D'Antona and Mazzitelli, 1993), and occurs at $t \sim< 0.1$ Gyr. Because the initial lithium abundance is very small, reaction (6) does not contribute appreciably to ϵ_N. An object older than 0.1 Gyr with detectable lithium in its atmosphere could be safely considered to be a BD. However, detection of such a low-abundance atom in such intrinsically faint objects presents a formidable observational challenge which has not yet been overcome.

20.4 Observational tests

20.4.1 Cluster luminosity functions

One of the best methods available at present to investigate properties of putative BD's in the solar vicinity is to examine low-luminosity objects in nearby galactic clusters. Such clusters are relatively young and have a known t as established by the evolution of their more massive members. One may use the function $L(M, t)$ as displayed in Fig. 1.3 to calculate the so-

https://doi.org/10.1017/S0252921100026488 Published online by Cambridge University Press

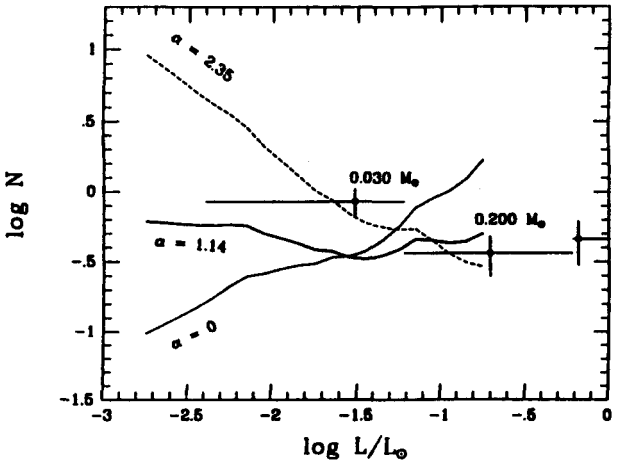

Fig. 20.4 Luminosity functions for ρ Oph for various values of α, compared with data from Comeron et al. (1993).

called luminosity function $N(L,t)$, where N is the number of objects within a given interval in $\log L$ at a given time t. To calculate N, one must also know the initial number of objects created within the cluster as function of M; this is given by the so-called initial mass function (IMF):

$$\xi(M)dM = CM^{-\alpha}dM \tag{7}$$

where $\xi(M)$ is the number of initial objects created within M and $M+dM$. The exponential dependence of ξ on M was discovered by Salpeter (1955), who also showed that $\alpha \approx 2.35$ for stars in the galaxy. It is at present uncertain whether a power law of the form of eq. (7) applies to BD's. Clearly, the proportion of the mass of the Galaxy comprised of BD's depends on the relevant value of α for the BD mass range. For VLM's (and possibly BD's) in the Hyades galactic cluster ($t = 0.6$ Gyr), Hubbard et al. (1990) found that the theory matched low-luminosity star counts best for $\alpha \approx 0$.

As is clear from Fig. 1.3, BD's are best detected in young clusters, when their luminosities are relatively elevated. Fig. 1.4 shows a comparison of star counts in the young galactic association ρ Oph ($t = 0.003$ Gyr; Comeron et al., 1993) with the theory of Burrows et al. (1993). In such a young cluster, deuterium burning is still important in the BD's. While the number of detected low-luminosity objects is still quite small, $\alpha = 1.14$ (Comeron et al., 1993) is a reasonable mean value for the BD-VLM mass range. This result, when added to $\xi(M)$ for objects more massive than VLM's, implies that at most 1/3 of the mass of the Galaxy is composed of BD's.

Figure 1.4 shows a very indirect test of the equation of state of BD's and VLM's. The primary influence of the equation of state on this plot is via its effect on the radii of the metallic-hydrogen objects, and on their

https://doi.org/10.1017/S0252921100026488 Published online by Cambridge University Press

thermal properties such as heat capacities and thermonuclear reaction rates. However, of equal importance are the atmospheric opacities which regulate the escape of interior heat, and the value of α.

20.4.2 Luminosity of giant planets

With the exception of Uranus, the solar system's giant planets have measurable intrinsic luminosities. These were determined with considerable precision by experiments on the Voyager spacecraft after encounters with all four bodies during the previous decade (Pearl et al., 1991). Values of both the intrinsic luminosity L and the specific luminosity (L/M) are given in Table 1.2. The theory of giant-planet luminosity is developed by integrating eq. (3) over t (after setting $\epsilon_N = 0$), thus determining the time interval required for the planet's luminosity to decline to the present observed value. This can be compared with the known ages of these planets ($t = 4.6$ Gyr). In the case of Jupiter and Saturn, the luminosities are governed by the thermal properties of hydrogen, and the most recent calculation of $L(t)$ for these objects (Saumon et al, 1992) has made use of the Plasma Phase Transition (PPT) theory of Saumon and Chabrier (1989, 1991, 1992). The calculation finds that interior adiabats in both Jupiter and Saturn cross the PPT during their evolution, at an interior point where $P \approx 1$ Mbar. The evolutionary age of the planet t_E is defined by the value of t for which the planet's luminosity drops to the value given in Table 1.2. For Jupiter, the theory gives $t_E = 5$ Gyr, but for Saturn $t_E = 2.5$ Gyr. Thus Jupiter's heat flow is in accordance with the latest equation of state of hydrogen and eq. (3), but Saturn's is not. The traditional explanation of the discrepancy for Saturn is that additional gravitational energy is liberated in Saturn's interior if helium becomes immiscible in hydrogen over part of the pressure-temperature range traversed in Saturn's interior (Stevenson and Salpeter, 1977). In this case helium droplets would form and sink to deeper layers in Saturn, liberating gravitational energy. Eq. (3) must be modified to take this mechanism into account (Hubbard and Stevenson, 1984). While the theory of helium-hydrogen phase separation in Saturn is as yet not fully quantitative, it does predict the substantial depletion of helium which is observed in Saturn's atmosphere (Conrath et al., 1984).

In the case of Uranus and Neptune, the equation of state is dominated by heavier materials than hydrogen or helium, as we discuss below. The most relevant quantity for the evolution of a giant planet's luminosity is its interior specific heat at constant volume per unit mass, C_V. Neglecting ϵ_N

https://doi.org/10.1017/S0252921100026488 Published online by Cambridge University Press

Table 20.2. *Measured luminosity and specific luminosity of GP's*

	$L/L_\odot$	L/M (10^{-11} W/kg)
Jupiter	0.9×10^{-9}	18
Saturn	0.2×10^{-9}	15
Uranus	$< 0.002 \times 10^{-9}$	< 0.8
Neptune	0.01×10^{-9}	3

and any effects of immiscibility, eq. (3) can be schematically expressed as

$$-C_V \frac{dT}{dt} \approx \left\langle \frac{L}{M} \right\rangle \tag{8}$$

where dT/dt is the time rate of change of the mean temperature T, and $\langle L/M \rangle$ is the specific luminosity.

One may estimate $C_V \approx 3k/Am$, where A is the mean atomic weight of the planet's interior material in amu. For Jupiter and Saturn, $A \approx 1$, while for Uranus and Neptune, $A \approx 5$. Thus according to eq. (8), Uranus and Neptune should cool more rapidly than Jupiter and Saturn because their average interior C_V is substantially lower. Yet, paradoxically, the estimated C_V is large enough to permit t_E for both Uranus and Neptune to greatly exceed their present age. The resolution of this paradox probably does not depend on some poorly understood property of the equation of state. Rather, it may be produced by large chemical gradients in the interiors of these hydrogen-depleted planets, which may have the effect of greatly impeding interior heat transport, especially in Uranus (Hubbard et al., 1994).

20.4.3 Giant planet interior structure

Determination of the interior structure of the giant planets in the solar system proceeds somewhat differently from the approach taken for BD's. Much more detailed constraints are available, but the solar system giant planets are also somewhat altered from pure solar composition (substantially altered in the case of Uranus and Neptune), and thus do not cleanly constrain the hydrogen equation of state. In fact, modeling studies have been directed toward accurate determination of the Z-component of Jupiter, Saturn, Uranus, and Neptune by comparing their inferred interior pressure-density profile with that of pure hydrogen.

The gravitational potential $V(\mathbf{r})$ within a planet satisfies Poisson's equa-

https://doi.org/10.1017/S0252921100026488 Published online by Cambridge University Press

tion ($\mathbf{r}$ is a vector from the planet's center of mass to the point of observation, and G is the gravitational constant),

$$\nabla^2 V = -4\pi G\rho \tag{9}$$

while if the planet is in hydrostatic equilibrium and rotates on cylinders, the equation of hydrostatic equilibrium can be written

$$\nabla P = \rho \nabla U \tag{10}$$

where $U = V + Q$ is a generalized total potential, composed of V and a rotational potential Q. Since the rotation of all four giant planets is observed to be axially symmetric and north-south symmetric, generally consistent with rotation on cylinders, we may assume that Q likewise has these symmetries. It follows that the overall planetary structure $\rho(\mathbf{r})$ is also axially symmetric and north-south symmetric, as is $V(\mathbf{r})$. Under these conditions, $V(\mathbf{r})$ exterior to the planet can be expanded in a form with the corresponding symmetry:

$$V = \frac{GM}{r}\left[1 - \sum_{\ell=1}^{\infty} J_{2\ell}\left(\frac{R}{r}\right)^{2\ell} P_{2\ell}(\cos\theta)\right] \tag{11}$$

where r is the magnitude of $\mathbf{r}$, and θ is the angle that $\mathbf{r}$ makes to the rotation axis. In eq. (11), the dimensionless coefficients $J_{2\ell}$ represent the response of the planet to the rotational potential Q, and they are a direct constraint on the interior equation of state $P(\rho)$, via the equation of hydrostatic equilibrium. Their value obviously depends on the choice of normalizing radius, R. For the giant planets, R is defined to be the equatorial radius of a surface at one bar pressure.

If the planet rotates as a solid body with period τ_S, one has

$$Q = \frac{4\pi^2 r^2}{3\tau_S^2}\left[1 - P_2(\cos\theta)\right] \tag{12}$$

and in this case one can show that $J_2 \propto Q$, $J_4 \propto Q^2$, etc. Although for none of the four giant planets do the atmospheric features rotate with any unique period τ_S, their magnetic field configurations rotate with a well-defined periods. It is the latter period which is taken to define τ_S, a period which corresponds to the deep interior of the planet.

All of the fundamental parameters constraining the interior equation of state of the four giant planets are presented in Tables 1.3 and 1.4.

Although attempts have been made to solve an inverse problem by inferring the interior equation of state from a knowledge of a giant planet's $J_{2\ell}$ and its Q, such inverse solutions are not well constrained with the limited

Table 20.3. *Parameters constraining interior structure of Jupiter and Saturn [$M_\oplus = 5.98 \times 10^{27}$ g = mass of the earth]*

	Jupiter	Saturn
M ($M_\oplus$)	317.735	95.147
R (km)	71492 ± 4	60268 ± 4
τ_S (hr)	9.92492	10.65622
$J_2(R) \times 10^6$	14697 ± 1	16331 ± 18
$J_4(R) \times 10^6$	-584 ± 5	-914 ± 38
$J_6(R) \times 10^6$	31 ± 20	108 ± 50

Table 20.4. *Parameters constraining interior structure of Uranus and Neptune*

	Uranus	Neptune
M ($M_\oplus$)	14.53	17.14
R (km)	25559 ± 4	24764 ± 20
τ_S (hr)	17.24 ± 0.01	16.11 ± 0.05
$J_2(R) \times 10^6$	3516 ± 3	3538 ± 9
$J_4(R) \times 10^6$	-31.9 ± 5	-38 ± 10

number of $J_{2\ell}$ that are available, together with relatively large error bars on the higher-degree terms. In practice, the modeling has proceeded by assuming that the planet is a barotrope (i.e., has a unique $P(\rho)$ relation throughout its interior). The equation of hydrostatic equilibrium is then integrated, for a specified function Q, to obtain a model planet of prescribed M. A satisfactory $P(\rho)$ must yield a model with the observed R and $J_{2\ell}$.

Since the equation of state $P(\rho, T)$ also depends on T, one needs a relation $T(\rho)$ or $T(P)$ to obtain the barotrope. Because of the interior heat flow in BD's and GP's, these bodies remain fully convective, even at the low luminosity values given in Table 1.2. If the convection is efficient, as is certainly the case for BD's as well as for chemically homogeneous GP's, the appropriate $T(P)$ is an adiabatic relation between temperature and pressure, which is uniquely specified by the starting temperature of the adiabat at some observationally accessible portion of the object's convective atmosphere.

Figure 1.5 shows adiabatic relations for $T(\rho)$, for solar composition, and for four different starting temperatures. The BD starting temperature is taken to be 550 K at $P = 10$ bar, as given in Table 1.1, while the starting

https://doi.org/10.1017/S0252921100026488 Published online by Cambridge University Press

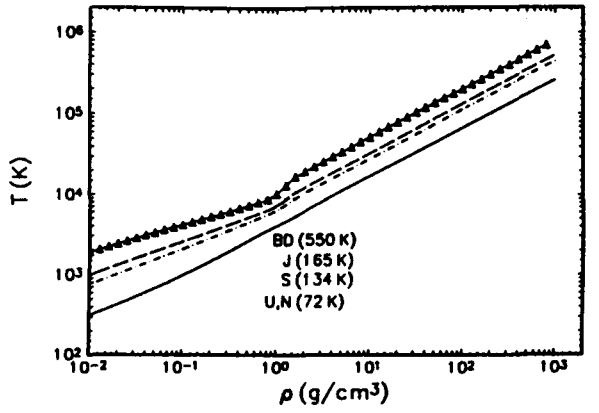

Fig. 20.5 Adiabats for (top to bottom) a BD, Jupiter, Saturn, and Uranus-Neptune.

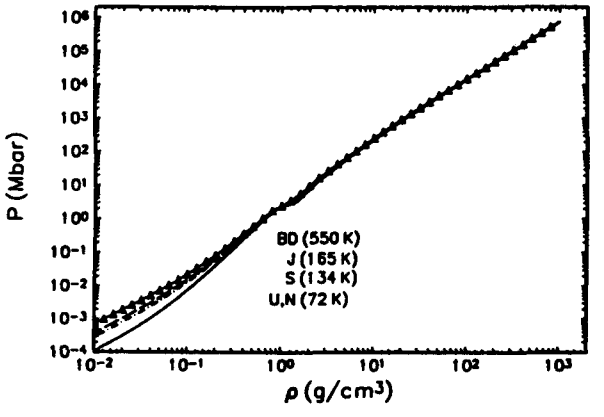

Fig. 20.6 The same adiabats as in Fig. 1.5, but on the P-ρ plane.

temperatures for the giant planets are evaluated at $P = 1$ bar, respectively for Jupiter (165 K), Saturn (134 K), and a common Uranus-Neptune adiabat (72 K). Figure 1.6 shows the same adiabats on the P-ρ plane. As this figure shows, in this range of adiabatic temperatures, the $P(\rho)$ relation is significantly changed by temperature effects by only for $\rho \sim< 1$ g cm^{-3}, outside the domain of stability of metallic hydrogen.

As is clear from Fig. 1.2, a chemically-homogeneous solar composition $P(\rho)$ relation cannot produce a satisfactory model of Uranus or Neptune. In fact, such a model fails to reproduce the $J_{2\ell}$ of Jupiter and Saturn as well. Figures 1.7 and 1.8 show $P(\rho)$ and $T(\rho)$ relations for the same BD model as given in Table 1.1, together with GP models which agree with the data of Tables 1.3 and 1.4.

As is made clear in Fig. 1.9, the four giant planets differ substantially from solar composition in their deep interiors. The equation of state for Jupiter follows the BD equation of state most closely, deviating toward a

https://doi.org/10.1017/S0252921100026488 Published online by Cambridge University Press

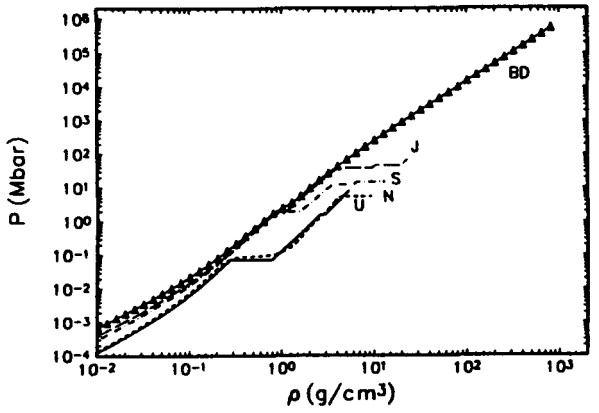

Fig. 20.7 The empirical equations of state for the four giant planets, compared with the equation of state for the BD model given in Table 1.1. The rightmost points for each object give values at the center.

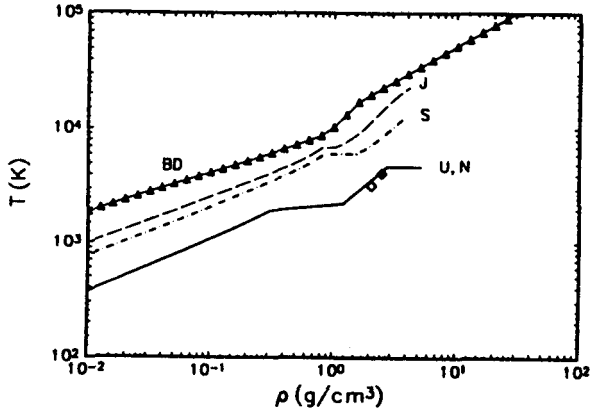

Fig. 20.8 Temperature profiles corresponding to the models shown in Fig. 1.7. For Uranus and Neptune, the ***diamonds*** show experimental points measured in dynamical shock compression experiments on synthetic Uranus material.

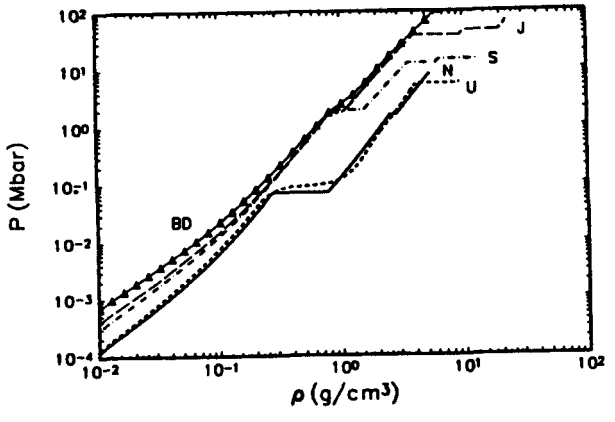

Fig. 20.9 An enlarged view of the GP models shown in Fig. 1.7.

https://doi.org/10.1017/S0252921100026488 Published online by Cambridge University Press

higher-density profile only in a small innermost ice or rock-ice core. By ice, we mean a material composed of the molecules H_2O, CH_4, and NH_3 in solar proportions, not necessarily with intact molecules, and not necessarily in the solid phase. For solar composition proportions of C, N, and O, the corresponding fractions are 56.5% H_2O, 32.5% CH_4, and 11% NH_3 by mass.

In Saturn, the deviation from the BD equation of state begins in the metallic-hydrogen region. The enhanced density of Saturn in the region is interpreted as being caused by enrichment of helium due to immiscibility in metallic hydrogen, and possible enrichment of the ice component as well (Chabrier et al., 1992).

Figure 1.9 shows that Uranus and Neptune have very similar interior equations of state. Satisfactory models for both planets have outer hydrogen-helium envelopes which extend to a maximum pressure of ~ 0.1 Mbar, below which point the equation of state very closely follows the $P(\rho)$ curve for ice (between $P \sim 0.1$ Mbar and 8 Mbar. A small rocky core may exist in either Uranus or Neptune, but is not required to fit the data.

Uranus and Neptune are composed primarily of ice, a substance which is accessible to laboratory shock compression experiments in the relevant pressure range. These experiments have been carried out on "synthetic Uranus", a solution of water, ammonia, and isopropanol with mole fractions of 0.71, 0.14, and 0.15 respectively, up to a pressure of 2.2 Mbar (Hubbard et al., 1991). In the limit of high pressure, this material should behave identically with solar proportions of H_2O, CH_4, NH_3. Figure 1.10 shows theoretical adiabats for mixtures of hydrogen-helium (in solar proportions) with ice, together with the shock data on "synthetic Uranus". All of the adiabats are computed for a starting temperature appropriate to Uranus or Neptune, and assume constant chemical composition. The left-most adiabat (marked $\odot$) is for pure hydrogen and helium in solar proportions. The next adiabat to the right (marked 0.2) represents a mixture of the solar-composition adiabat with 0.2 mass fraction of ice, etc., ending with an adiabat of pure ice composition. The diamond symbols shown on Fig. 1.10 show the shock compression data for "synthetic Uranus" of Nellis et al. (1988). Open diamonds represent data from single shock compression, while solid diamonds are data from double shock compression. The two points marked with larger symbols are points for which the temperature was simultaneously measured; the latter data are shown in Fig. 1.8 as well.

Finally, Fig. 1.11 shows the curves and data points of Fig. 1.10, superimposed on interior models of Uranus (dashed curve) and Neptune (solid curve). Open squares and circles show transition points in two alternative

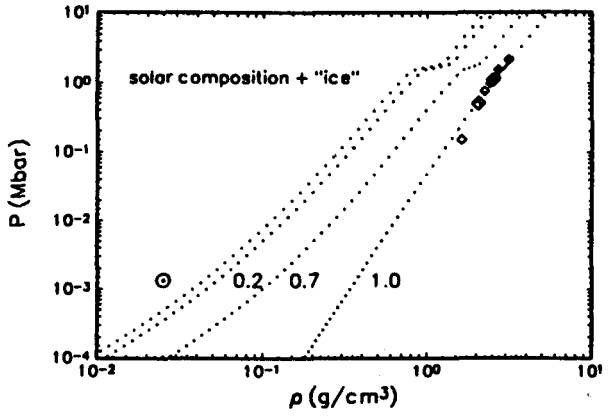

Fig. 20.10 Theoretical adiabats for mixtures of H and He in solar proportions, mixed with ice. *Diamonds* show shock compression data on ice.

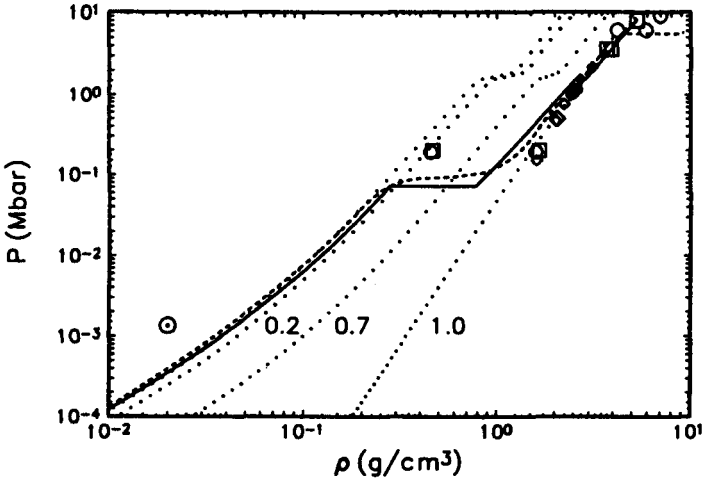

Fig. 20.11 Interior models of Uranus and Neptune.

interior models of Neptune calculated by Zharkov and Gudkova (1991); in the latter models, the hydrogen-helium envelope extends to about 0.2 Mbar.

20.5 Conclusion

The properties of a broad range of astrophysical objects, ranging from VLM's (masses $\sim 0.1 M_\odot$) to giant planets (masses $\sim 0.001 M_\odot$) can be investigated within the framework of a general equation of state for a mixture of hydrogen and helium. For the more massive objects, confrontation between theory and data comes primarily from a comparison of the predicted spectral properties of photons emitted from BD atmospheres, as a function of their interior thermal properties and age, with the (sparse) observational data set.

https://doi.org/10.1017/S0252921100026488 Published online by Cambridge University Press

For the giant planets within our solar system, it is possible to study not only the relation between intrinsic luminosities and interior thermal state, but also the relation between the gravitational potential coefficients $J_{2\ell}$ and the interior $P(\rho)$ relation. A further constraint on the interior equation of state comes from the $M(R)$ relation. A primary result of this study is that, commencing at masses comparable to that of Jupiter, giant planets form in a process which tends to lose some of the hydrogen-helium component as the planet accretes. As the object's mass decreases, ever more hydrogen-helium is lost, such that objects in the mass range of Uranus and Neptune contain only a small fraction ($\sim$ few % by mass) of hydrogen-helium.

In the mass range of Uranus and Neptune, typical central pressures reach only a few Mbar. Likely interior material (ice) is susceptible to experimental determination of its equation of state in this pressure range. Thus, theory can be at least partially replaced with experiment when equations of state are tested for the lowest mass giant planets.

This work was supported in part by NASA Grant NAGW-1555 and by NSF Grant INT-8907133.

References

Boss A.P., in *Astrophysics of Brown Dwarfs* (M.C. Kafatos, R.S. Harrington, S.P. Maran, eds.), Cambridge Univ. Press, pp. 206-211, (1986)
Burrows A., Hubbard W.B., Lunine J.I., *Astrophys. J.* **345**, 939, (1989)
Burrows A., Hubbard W.B., Saumon D., Lunine J.I., *Astrophys. J.* **406**, 158, (1993)
Chabrier G., Saumon D., Hubbard W.B., Lunine J.I., *Astrophys. J.* **391**, 817, (1992)
Comeron F., Rieke G.H., Burrows A., Rieke M.J., *Astrophys. J.* **416**, 185, (1993)
Conrath B.J., Gautier D., Hanel R.A., Hornstein J.S., *Astrophys. J.* **282**, 807, (1984)
D'Antona F., Mazzitelli I., *Astr. J. Suppl.*, in press, (1993)
Dyson F., *Ann. Phys.* **63**, 1, (1971)
Hubbard W.B., Burrows A., Lunine J.I., *Astrophys. J.* **358**, L53, (1990)
Hubbard W.B., Nellis W.J., Mitchell A.C., Holmes N.C., Limaye S.S., McCandless P.C., *Science* **253**, 648, (1991)
Hubbard W.B., Pearl J.C., Podolak M., Stevenson D.J., in *Neptune and Triton* (D. Cruikshank, ed.) Univ. of Arizona Press, in press, (1994)
Hubbard W.B., Stevenson D.J., in *Saturn* (T. Gehrels, M.S. Matthews, eds.), Univ. of Arizona Press, pp. 47-87, (1984)
Magazzù A., Martin E.L., Rebolo R., *Astrophys. J.* **404**, L17, (1993)
Nellis W.J., Hamilton D.C., Holmes N.C., Radousky H.B., Ree F.H., Mitchell A.C., Nicol M., *Science* **240**, 779, (1988)
Pearl J.C., Conrath B.J., *J. Geophys. Res.* **96**, 18921, (1991)
Salpeter E.E., *Astrophys. J.* **121**, 161, (1955)
Saumon D., Chabrier G., *Phys. Rev. Lett.* **62**, 2397, (1989)

Saumon D., Chabrier G., *Phys. Rev. A* **44**, 5122, (1991)
Saumon D., Chabrier G., *Phys. Rev. A* **46**, 2084, (1992)
Saumon D., Hubbard W.B., Chabrier G., Van Horn H.M., *Astrophys. J.* **391**, 827, (1992)
Stevenson D.J.,*Phys. Rev.* **12B**, 3999, (1975)
Stevenson D.J., Salpeter E.E., *Astrophys. J. Suppl.* **35**, 221, (1977)
Zharkov V.N., Gudkova T.V., *Ann Geophysicae* **9**, 357, (1991)